The role of desmoplakin for neuronal function in the dentate gyrus and anxiety-related behavior

Keisuke Otsubo[1,3], Naoko Sakashita[1,3], Yuki Nishimoto[1,3], Yo Sato[1], Katsunori Kobayashi[2], Kanzo Suzuki[1], Eri Segi-Nishida[1,4,*]

[1]Department of Biological Science and Technology, Faculty of Advanced Engineering, Tokyo University of Science, Tokyo, Japan

[2]Department of Pharmacology, Graduate School of Medicine, Nippon Medical School, Tokyo, Japan

[3] These authors equally contributed to this work

[4] Lead Contact

*Correspondence to:

Eri Segi-Nishida,

6-3-1 Niijuku, Katsushika-ku, Tokyo, Japan, 125-8585

Email: eri.segi.nishida@rs.tus.ac.jp

Running title: Role of desmoplakin in DG

Summary

Desmoplakin (Dsp) is a component of desmosomal cell-cell junctions. In the central nervous system, Dsp is specifically expressed in the hippocampal dentate gyrus (DG). However, it is unclear how Dsp impacts hippocampal function and its related behaviors. In this study, we provide evidence that Dsp in the DG maintains hippocampal functions, including neuronal activity and adult neurogenesis, and contributes to anxiolytic-like effects using an adeno-associated virus knockdown system in male mice. Dsp knockdown in the DG resulted in a lowered expression of an activity-dependent transcription factor FosB and reduction of serotonin responsiveness at the DG mossy fiber synapses. In addition, the suppression of Dsp impairs adult neurogenic processes in the DG. Moreover, DG-specific Dsp knockdown mice showed an increase in anxiety-like behaviors. Taken together, this research suggests that Dsp in the DG may function as a regulator to maintain proper neuronal activation and contribute to the adaptation of emotion-related behavior.

Introduction

Desmosomes are adhesive intercellular junctions that provide strong adhesion between cells and are abundant in tissues exposed to mechanical stress, such as the heart and skin. Mutations in these factors cause skin and heart vulnerability (Kowalczyk and Green, 2013). Desmosomal components comprise transmembrane cadherins, such as desmoglein and desmocollin, and intracellular proteins, such as plakoglobin, plakophilin, and desmoplakin (Dsp) (Garrod and Chidgrey, 2008; Broussard et al., 2015). Dsp is a family of plakin proteins that interacts with the cadherin/plakoglobin/plakophilin complex through the N-terminal domain and with an intermediate filament cytoskeleton through the C-terminal domain (Delva et al., 2009). In addition to mediating cell-to-cell adhesion, desmosomes function as cell signaling regulators involved in cell proliferation and differentiation (Johnson et al. 2014). In particular, Dsp is involved in processes such as gene expression, differentiation, and microtubule dynamics, indicating its diverse biological functions in addition to its function as an adhesion component (Bendrick et al., 2019; Dubash et al., 2016; Lombardi et al., 2016; Patel et al., 2014).

In the central nervous system, Dsp is specifically expressed in the hippocampal dentate gyrus (DG) in the brain (Yamasaki et al., 2008). The DG gates the flow of neocortical information into the hippocampal CA3 region and is one of the few areas of the mammalian brain where adult neurogenesis occurs (Drew et al., 2013; Zhao et al., 2008). It has been reported that Dsp is characterized as a molecular maker for neuronal maturation in the DG of hippocampus (Kobayashi et al., 2010). The expression level of *Dsp* in the DG increases with postnatal development, similarly to the patterns of other DG maturation markers, calbindin and tryptophan-2,3-dioxygenase 2 (Tdo2). Dsp transcription is directly regulated by Bcl11b, a transcription

factor that plays an important role in postnatal development of the DG (Simon et al., 2012). Forebrain neuron-specific knockout of Dsp in Emx1-Cre mice impairs progenitor proliferation and neuronal differentiation at 14 days postnatal age, indicating that Dsp contributes to the development of dentate granule neurons (Simon et al., 2012). However, whether Dsp regulates the function of dentate mature granule neurons and affects the process of adult neurogenesis in the DG remain unclear.

The hippocampus is a limbic structure implicated in the regulation of stress and pathophysiology/treatment of anxiety and depression (Segi-Nishida and Suzuki, 2022). We have previously demonstrated that long-term antidepressant treatment suppresses the expression of *Dsp* in the DG (Kobayashi et al., 2010; Imoto et al., 2017), indicating that Dsp plays a key role in emotion-related behaviors in the DG. Nevertheless, whether Dsp in the DG during adulthood is involved in emotion-related behaviors such as depression and anxiety is unclear.

In this study, we investigated the effect of Dsp knockdown in the DG on neuronal activation, adult hippocampal neurogenesis, and emotion-related behaviors using an adeno-associated virus (AAV) knockdown system in mice. We found that Dsp in the adult hippocampal DG maintains the function of dentate granule neurons, regulates neuronal differentiation during adult neurogenesis, and behaviorally contributes to anxiolytic-like effects.

Materials and Methods

Experimental animals

Seven-to-eight-week-old male C57BL/6N mice (23–25 g) were purchased from Japan SLC (RRID5295404; Hamamatsu, Japan). The mice were housed in groups of six per cage (32 cm length × 11 cm width × 13.5 cm height). All the mice were housed under standard conditions (temperature: 24 ± 2 °C, humidity: 55% ± 5%) with a 12 h light/dark cycle and *ad libitum* access to water and food (MR standard, Nosan Corporation, Yokohama, Japan). The weight gain of each mouse was recorded during the experiments to monitor their physical condition. All mice were habituated for longer than one week before the experimental procedures were performed. A total of 132 mice were used in this study (control animals, n=14; ECS-treated animals, n=6; fluoxetine-treated animals, n=7; AAV control miRNA infected animals, n=52; AAV Dsp miRNA infected animals, n=53). Animal use and procedures were conducted in according the Tokyo University of Science regulations on animal care and use in research and were approved by the Animal Care and Use Committee of Tokyo University of Science (approval numbers K20009, K21007, and K22007).

AAV preparation and hippocampal administration

AAVs (serotype rh10) expressing artificial microRNAs (miRNAs) targeting Dsp or control miRNAs with Emerald Green Fluorescent Protein (EmGFP) under the EF1α promoter were generated as follows: We designed the sequences for artificial microRNAs for Dsp according to the BLOCK-iT RNAi Designer website (Thermo Fisher Scientific). First, the DNA fragment encoding miRNA for *Dsp* (5'-TGC TGT TGA GAT GGA CAT CAA TGC ACG TTT TGG CCA CTG ACT GAC GTG CAT TGG TCC ATC TCA A-3' and 5'-CCT GTT GAG ATG GAC CAA TGC ACG TCA

GTC AGT GGC CAA AAC GTG CAT TGA TGT CCA TCT CAA C-3') was subcloned into pcDNA6.2-GW-EmGFP-miR using BLOCK-iT Pol II miR RNAi Expression Vector Kit (Invitrogen). The EmGFP and Dsp miRNA fragments were amplified by PCR from this vector and inserted between the KpnI and EcoRV sites of the pAAV-EF1α-DIO EYFP vector (#27056; Addgene). The resulting plasmid was named pAAV-EF1α-EmGFP-miR-Dsp. The DNA fragment encoding control microRNA (5′-TGC TGA AAT GTA CTG CGC GTG GAG ACG TTT TGG CCA CTG ACT GAC GTC TCC ACG CAG TAC ATT T-3′ and 5′-CCT GAA ATG TAC TGC GTG GAG ACG TCA GTC AGT GGC CAA AAC GTC TCC ACG CGC AGT ACA TTT C-3′), which can form a hairpin structure processed into mature microRNA but is predicted not to target any known vertebrate gene, was used to generate an AAV vector expressing control microRNA. TheBLOCK-iT Pol II miR RNAi Expression Vector Kit was used instead of those encoding Dsp miRNA. AAV particles were produced using the previously described procedure with minor modifications (Shinohara et al., 2018). Briefly, the AAVrh10 expression plasmid (Addgene #112866), pHelper vector (#240071, Agilent Technologies, Santa Clara, CA), and the constructed AAV-vector plasmid were transfected into AAV-293 cells (#240073, Agilent) using Lipofectamine 2000 (Thermo Fisher Scientific). Transfected AAV-293 cells were collected 72 h after transfection and resuspended in artificial cerebrospinal fluid. The cell suspensions were freeze-thawed three times. Cell debris was eliminated by centrifugation at 10,000 × g for 10 min and the supernatant containing the virus was collected. The viral suspension was incubated with benzonase (Merck Millipore, Burlington, MA, USA) to degrade residual DNA. The prepared AAV solution was aliquoted and stored at -80 °C. The AAV titer was quantified using PCR (5′-TGA GTC ACC CAC ACA AAG GA-3′ and 5′-CCA AGC TGG CCT AAC TTC AG-3′) after proteinase K treatment (Merck

131 Millipore). Under anesthesia with a mixture of medetomidine (0.3 mg/kg, ZENOAQ,
132 Japan), midazolam (4 mg/kg, Sandoz, Japan), and butorphanol (5 mg/kg, Meiji, Japan),
133 the mouse brain was fixed with stereotaxic instruments (Narishige, Tokyo, Japan). An
134 AAV solution of 500 nL per injection site (5.0×10^8 copies) was bilaterally injected
135 into the DG using a PV-820 Pneumatic PicoPump (World Precision Instruments,
136 Hessen, Germany) through a glass micropipette made with a PN-30 micropipette puller
137 (Narishige). The stereotaxic coordinates were targeted to the ventral DG: 3.2 mm
138 posterior to the bregma, 2.7 mm lateral to the midline, and 3.0 mm ventral to the skull
139 surface at the bregma, according to the mouse brain atlas (Paxinos and Franklin, 2012).
140 Data were excluded from the analysis if fluorescence was not observed in the DG.
141
142 **Electroconvulsive stimulation and drug treatment**
143 Bilateral ECS (current, 25–35 mA; shock duration, 1 sec; frequency, 100 pulse/sec;
144 pulse width, 0.5 msec) was administered with a pulse generator (ECT Unit; Ugo Basile,
145 VA, Italy) to mice as described previously (Imoto et al., 2017). ECS was administered
146 4 times a week. Fluoxetine hydrochloride (LKT Labs, St. Paul, MN, USA) was
147 dissolved in drinking water and orally applied at a dose of 22 mg/kg/day for 4 weeks
148 as described previously (Kobayashi et al., 2010).
149
150 **RNA extraction and real-time PCR**
151 Seven to eight weeks after AAV infection, the mice were decapitated under deep
152 anesthesia, coronal brain slices (1 mm) were cut using a tissue slicer, and the DG of the
153 hippocampus was dissected. Total RNA was extracted using the Reliaprep RNA Cell
154 Miniprep System (Promega, Madison, WI, USA) and reverse transcribed using
155 ReverTra Ace (Toyobo, Osaka, Japan). Subsequent, real-time PCR was performed

156 using the StepOne system (Applied Biosystems, Foster City, CA) and Thunderbird
157 SYBR qPCR mix (Toyobo). The expression levels of each gene were quantified using
158 standardized external dilutions. The relative expression levels of the target genes were
159 normalized to those of 18S rRNA or *Gapdh*. The specificity of each primer set was
160 confirmed by melt-curve analysis, and the product size was examined using gel
161 electrophoresis. Table 1 summarizes the primer sequences for each gene.
162

163 **Electrophysiological analysis**

164 Mice were decapitated under deep anesthesia 7–8 weeks after AAV infection, and both
165 hippocampi were isolated. Transverse hippocampal slices (380 μm) were cut in ice-cold
166 saline using a tissue slicer (7000smz, Campden Instruments Ltd., Leics, UK). The slices
167 were then incubated for 30 min at 30 °C and maintained in a humidified interface-
168 holding chamber at room temperature before use. Intense GFP fluorescence in the DG
169 and the mossy fiber (MF) tract was confirmed, and electrophysiological recordings
170 were performed as described (Kobayashi et al., 2010, 2020). Electrophysiological
171 recordings were made in a submersion-type chamber maintained at 27.0–27.5 °C and
172 superfused at 2 mL/min with recording saline composed of (in mM): NaCl, 125; KCl,
173 2.5; NaH2PO4, 1.0; NaHCO3, 26.2; glucose, 11; CaCl2, 2.5; MgCl2, 1.3 (equilibrated
174 with 95% O2 / 5% CO2). Field excitatory postsynaptic potentials (EPSPs) arising from
175 the MF synapses were evoked by stimulating the dentate granule cell layer with bipolar
176 tungsten electrodes and were recorded from the stratum lucidum of CA3 using a glass
177 pipette filled with 2 M NaCl. The amplitude of field EPSPs was measured with a 0.5-
178 ms window positioned at 70–80% of the peak of the baseline field EPSPs. More than
179 85% block of EPSP by an agonist of group II metabotropic glutamate receptors
180 (2*S*,2'*R*,3'*R*)-2-(2',3'-dicarboxycyclopropyl) glycine (DCG-IV, 1 μM) was the criterion

181 used to identify MF input. A single electrical stimulation was delivered at a frequency
182 of 0.05 Hz. The initial slope of the EPSPs was measured through analysis. All
183 recordings were performed using a Multiclamp 700 B amplifier (Molecular Devices,
184 Sunnyvale, CA, USA), filtered at 2 kHz, and stored on a personal computer via an
185 interface (digitized at 10 kHz). Data were obtained from distinct samples. Serotonin
186 hydrochloride was purchased from Sigma-Aldrich.
187
188 **Sample isolation for immunohistochemistry**
189 Five'-bromo-2'-deoxyuridine (BrdU, 150 mg/kg, Nacalai Tesque, Japan) was
190 intraperitoneally administered to mice once 2 h before sacrifice to evaluate cell
191 proliferation to label the dividing cells, or four times on 14 and 15 days (twice a day)
192 before sacrifice to evaluate cell survival.
193 For Dsp immunostaining, the mice were deeply anesthetized and transcardially
194 perfused with cold saline. The brains were then stored at -80°C until further use. Serial
195 fresh frozen sections (18 μm thick) were cut through the entire hippocampus using a
196 cryostat (Leica 1510, Leica Microsystems, Wetzlar, Germany) and stored at -80°C. For
197 other immunostaining procedures, mice were deeply anesthetized and perfused with
198 cold saline followed by 4% paraformaldehyde (Sigma-Aldrich) in 0.1 M phosphate
199 buffer (pH 7.4) and were post-fixed at 4 °C for 48 h. The brains were then cryoprotected
200 in 20% sucrose for 48 h and in 30% sucrose for 24 h and stored at -80°C until further
201 use. Serial sections (30 μm thick) were cut through the entire hippocampus using a
202 cryostat and stored in 30% glycerol and 30% ethylene glycol in 0.02 M phosphate
203 buffer (pH 7.4) at -20 °C until staining.
204
205 **Immunohistochemistry**

206 For Dsp/NeuN or Dsp/NeuroD1 immunostaining, fresh frozen sections were fixed with
207 100% methanol for 20 min at 4 °C. After fixation, the sections were washed with
208 phosphate-buffered saline (PBS), blocked using 10% equine serum in PBS, and
209 incubated with monoclonal mouse anti-Dsp (1:50; Progen, 61003, RRID:AB_2920666)
210 and rabbit anti-NeuN (1:500, Abcam, ab177487, RRID:AB_2532109) or rabbit anti-
211 NeuroD1 (1:500; Abcam, ab213725, RRID:AB_2801303) at 4 °C overnight. After
212 washing with PBS, the sections were incubated with donkey anti-mouse IgG antibody
213 conjugated to Alexa Fluor 488 (1:300; Thermo Fisher Scientific, RRID:AB_141607)
214 and donkey anti-rabbit IgG antibody conjugated to Alexa Fluor 555 (1:1000; Thermo
215 Fisher Scientific, RRID:AB_162543) for 60 min. The sections were then incubated with
216 4',6-diamidino-2-phenylindole (DAPI; 1:5,000; Merck Millipore) and covered with
217 Mowiol (Merck Millipore) after washing with PBS. Confocal images were taken using
218 Olympus FV3000. Single confocal images were shown for localization of Dsp. Anti-
219 Dsp and rabbit anti-mouse IgG antibody conjugated to Alexa 555 (1:300; Thermo
220 Fisher Scientific, RRID:AB_2535848) were used to confirm Dsp knockdown.

221 For FosB, NeuroD1, and doublecortin (DCX) immunostaining, the 30 μm thick
222 floating sections were washed with PBS and blocked using 10% equine serum
223 (SH30074; Cytiva) in PBS containing 0.3% Triton X-100 (PBST) at room temperature
224 for 60 min, followed by overnight incubation with rabbit anti-FosB (1:1000; Abcam,
225 ab184938, RRID: AB_2721123), rabbit anti-NeuroD1 (1:1000), rabbit anti-
226 doublecortin (DCX) (1:1000; Cell Signaling Technology, Danvers, MA, USA;
227 RRID:AB_561007) at 4 °C. For BrdU immunostaining, the floating sections were
228 incubated in 50% formamide in 2×saline sodium citrate buffer (SSC) for 2 h at 60 °C,
229 followed by incubation in 2 M hydrogen chloride at 37 °C for 30 min, and neutralized
230 with 0.1 M boric acid (pH 8.5) at room temperature for 10 min before blocking. After

231 blocking, the sections were incubated overnight with monoclonal rat anti-BrdU
232 (1:8000; Abcam, ab6326, RRID:AB_305426) at 4°C. After washing with PBST, the
233 sections were incubated with donkey anti-rabbit IgG antibody conjugated to Alexa
234 Fluor 555 (1:1000 for NeuroD1 and FosB immunostaining; Thermo Fisher Scientific,
235 RRID:AB_2535853) and donkey anti-rat IgG antibody conjugated to Alexa Fluor 555
236 (1:1000 for BrdU immunostaining; Abcam, RRID: AB_2813834) for 60 min. After
237 washing with PBST, the sections were incubated with DAPI (1:10,000) and mounted
238 on slides with Mowiol after washing with PBS. For DCX immunostaining, the sections
239 were incubated with biotinylated goat anti-rabbit IgG (1:200; Vector Laboratories Inc.,
240 Burlingame, CA, USA; BA1000, RRID: AB_2313606) for 60 min. The sections were
241 washed with PBST and incubated with the ABC Vectastain Kit (Vector), and antigen
242 detection was performed with 0.06% 3,3'-diaminobenzidine (Wako) staining. After
243 washing, the sections were mounted on slides using Entellan New (Merck Millipore).
244 Sections were photographed under a microscope (BZX-700, Keyence, Osaka, Japan).
245

246 **Quantification of BrdU-, NeuroD1-, DCX-, and FosB-positive cells**

247 Computer-assisted image analysis (ImageJ, NIH, Bethesda, MD, USA; QuPath,
248 Bankhead et al., 2017) was used for cell analysis. For quantification of FosB-positive
249 cells, three hippocampal sections with EGFP-expressing DG were photographed. The
250 number of FosB-positive cells was counted and presented as the number of cells per
251 10,000 μm^2 area in the granule cell layer of the DG. For BrdU-labeled cell
252 quantification, 6–8 hippocampal sections with EGFP-expressing DG were
253 photographed. To evaluate cell proliferation, the number of BrdU-positive cells was
254 counted in the subgranular zone (SGZ) and presented as the number of cells per 1,000
255 μm along the SGZ. To evaluate cell survival, the number of BrdU-positive cells in the

256 granule cell layer of the DG was counted and presented as the number of cells per
257 100,000 μm^2 of the granule cell layer. For NeuroD-positive cell quantification, four
258 hippocampal sections with EGFP-expressing DG were photographed. The number of
259 NeuroD1-positive cells in the SGZ was counted and presented as the number of cells
260 per 1,000 μm along the SGZ. For DCX-positive cell quantification, 2–3 hippocampal
261 sections with EGFP-expressing DG were photographed. DCX-positive cells in which
262 dendrites reached the molecular layer and underwent complex processes were
263 subcategorized as DCX-positive cells with long and branched dendrites. The total
264 number of DCX-positive and DCX-positive cells with long dendrites was counted in
265 the SGZ and presented as the number of cells per 100 μm along the SGZ.
266
267 **Behavioral experiments**
268 The mice were habituated to the testing room for at least 30 min before the behavioral
269 test. During the test, the movement of each mouse was recorded using a digital video
270 camera. All records were stored and analyzed using the SMART 3.0 video tracking
271 software (Panlab, Barcelona, Spain, RRID: SCR_002852). The apparatus was
272 thoroughly cleaned with 70% ethanol after the removal of each mouse.
273 The open field test (OFT) was performed for 10 min using an apparatus
274 composed of opaque white walls and a floor (50 cm × 50 cm × 20 cm) illuminated at
275 an intensity of 80 lux in the center of the floor. Each mouse was placed in the center of
276 an open-field arena, and locomotor activity was recorded for 10 min. The total distance
277 moved, relative time spent in the central zone, and entry time into the central zone were
278 measured. The floor was divided into 25 squares, and the four central squares were
279 defined as the central zone.

The forced swim test (FST) was performed in a cylindrical container (13 cm diameter, 25.5 cm height) filled with water to a height of 18 cm. Water (23–25 °C) was replaced between the trials. The FST was performed and recorded for 10 min using a digital video camera. The duration of immobility was then quantified.

The spontaneous locomotor activity (LMA) test was performed in a transparent home cage without bedding (20 cm length × 12.5 cm width) over 60 min. The total distance moved during the last 30 min was tracked.

The compartment social interaction test (SIT) was performed in an SIT apparatus (LE894T, Panlab) consisting of three chambers (42 cm × 60 cm × 22 cm) and two partitions (5.5 cm × 0.15 cm × 17 cm). Each mouse was placed in the middle chamber and allowed to explore the chamber freely for 5 min. Immediately after habituation, an unfamiliar mouse (a 7–8-week-old male C57BL/6N mouse) was introduced into one of the two side chambers enclosed in a wire cage. An identical empty wire cage was placed on the opposite side of the chamber. After placement, the side doors were opened simultaneously, and the test mouse was allowed to explore the entire three-chamber arena for 10 min. The time spent in each compartment was measured.

An elevated plus maze (EPM) test was performed in an EPM apparatus (EPM-X, Muromachi Kikai, Japan) consisting of two open arms (30 cm × 6 cm, 40 lux) and two closed arms (30 cm × 6 cm × 15 cm, 20 lux) extending from a central platform (6 cm × 6 cm). The maze was elevated to 40 cm above the floor. Each mouse was placed in the center of the maze, facing the open arm, and allowed to explore freely for 10 min. The total distance and time spent in the open arms were measured.

Statistical analyses

All data are presented as the mean ± standard error of the mean. Statistical analyses were performed using an unpaired Student's *t*-test, Welch's *t*-test, the Mann–Whitney U test, or two-way analysis of variance (ANOVA). Statistical significance was set at $P < 0.05$. Before performing *t*-test, normality of the data was examined using the Shapiro–Wilk test. If the data did not pass the normality test, a nonparametric test, the Mann–Whitney U test, was performed. We did not conduct a test for outliers. Detailed statistical data are presented in Table 2 (Table 2). All analyses were performed using the PRISM 9 software (GraphPad, San Diego, CA, USA).

313 ## Results

314 **Expression of Dsp in the hippocampal DG and its regulation by antidepressant**
315 **stimulation**

316 *Dsp,* a granule cell-specific maturation marker (Yamasaki et al., 2008; Kobayashi et al.,
317 2010), is highly and specifically expressed in the DG of the hippocampus of the central
318 nervous system (Fig. 1A, Allen Institute for Brain Science, 2004). However, the
319 localization of Dsp protein in the DG has not been fully investigated. Therefore, we
320 initially examined the cellular localization and cell type of Dsp expression.
321 Immunohistological analysis revealed that Dsp was highly expressed in the granule cell
322 layer and molecular layer in the DG compared to the CA1 region (Fig. 1B). Dsp
323 immunoreactivity signals were detected in NeuN-positive cells in the DG (Fig. 1C,
324 upper). However, Dsp signals were rarely existed in NeuroD1-positive neural
325 progenitors or immature neurons in the SGZ of the DG (Fig. 1C, lower, arrows). These
326 findings suggest that Dsp is expressed in mature granule neurons in the DG. Dsp
327 immunostaining was only observed after methanol fixation; therefore, the localization
328 of other neuronal markers such as an immature neuronal marker DCX was not
329 investigated.

330 Furthermore, we investigated whether Dsp expression was regulated by
331 antidepressant stimulation at the protein level. The expression of *Dsp* in the DG was
332 reduced by chronic administration of electroconvulsive seizure (ECS) or a selective
333 serotonin reuptake inhibitor (SSRI) (Fig. 1D), as previously reported (Imoto et al.,
334 2017). Immunohistological analysis confirmed that the cellular localization of Dsp was
335 reduced after repeated administration of ECS (Fig. 1E).

336

Dsp expression knockdown in the DG by an adeno-associated virus (AAV) carrying Dsp miRNA

To explore the role of Dsp in hippocampal function, we performed an AAV-mediated knockdown of Dsp in the DG. For this purpose, we generated AAVrh10 expressing EGFP and an artificial miRNA targeting Dsp mRNA (AAV-Dsp miRNA; Fig. 2A). The AAV rh10 serotype shows high transduction efficiency into granule cells in the DG (Sehara et al., 2022). Seven to eight weeks after the injection of AAV-Dsp or AAV-control miRNA into the DG, strong EGFP signals, which were co-expressed with miRNA, were observed in the molecular layer and granule cell layer in the DG and CA3 projection area (Fig. 2A, left). EGFP signals did not co-localize in DCX-positive cells in the DG (Fig. 2A, right), indicating that AAV-mediated gene transfer occurs primarily in mature granule neurons of the DG. *Dsp* mRNA expression significantly decreased in the AAV-Dsp miRNA group (Fig. 2B). Moreover, immunohistological analysis showed a decrease in Dsp immunoreactivity in the DG following AAV-Dsp miRNA injection (Fig. 2C), demonstrating that the sequence of artificial miRNAs targeting Dsp used in this study has the potential to knockdown Dsp expression.

Changes in activity- and mature-related marker expression in the DG and alteration of the sensitivity to serotonin at the MF synapse by Dsp knockdown

First, we examined the direct effect of Dsp knockdown on the activity of dentate granule neurons. FosB, including ΔFosB, is induced in response to many types of chronic stimuli and accumulates because of its high stability (Nestler et al., 1999; Lamothe-Molina et al., 2022). Consequently, we performed immunohistochemical analysis using an anti-FosB antibody to monitor neuronal activity in the DG under normal home-cage

361 conditions. FosB immunoreactivity in the granule cell layer of the DG significantly
362 decreased in the Dsp knockdown group (Fig. 2D).

363 Because Dsp is a granule cell-specific DG maturation marker (Yamasaki et al.,
364 2008; Kobayashi et al., 2010), we examined the expression of other markers, including
365 *Calb, Tdo2, Ntf3, and Il1r1* in the DG. The expression of *Calb, Tdo2,* and *Ntf3*
366 significantly increased in the DG of the Dsp knockdown group (Fig. 2E). These results
367 indicate that Dsp in the DG is involved in the regulation of neuronal activity and
368 expression of maturation markers.

369 Antidepressant treatments substantially change the physiological properties of
370 the synapses formed by DG output MFs onto CA3 pyramidal cells, concomitantly with
371 the reduction in Dsp expression (Kobayashi et al., 2010; Imoto et al., 2017).
372 Electrophysiological analyses of MF-CA3 synaptic transmission were then performed
373 using acute hippocampal slices (Fig. 3A). No significant changes in the ratio of field
374 EPSP to fiber volleys were observed (Fig. 3B), suggesting that the basal transmission
375 efficacy at the MF synapse was not altered by Dsp knockdown. Antidepressant
376 treatment attenuates the synaptic facilitation induced by repetitive stimulation and
377 augments serotonergic modulation at the MF synapse (Kobayashi et al., 2010; Imoto et
378 al., 2017; Kobayashi et al., 2020). Dsp knockdown did not change synaptic facilitation
379 after 1 Hz stimulation (Fig. 3C and D). Bath-applied serotonin induced the potentiation
380 of field EPSPs in the AAV control group (Fig. 3E), consistent with the findings of
381 previous studies. The magnitude of serotonin-induced potentiation was significantly
382 reduced in the Dsp knockdown group (Fig. 3E and F). Collectively, these findings
383 indicate that suppression of Dsp alters neuronal activity in the DG and sensitivity to
384 serotonin at the MF synapse.

385

386 **Changes in neurogenic activity in the DG by Dsp knockdown**

387 Adult hippocampal neurogenesis consists of proliferation, differentiation, and survival
388 and is regulated by various factors, including signals from adjacent mature granule
389 neurons in the DG (Kempermann et al., 2015). Since the above results suggest that Dsp
390 regulates neuronal activation in the DG, we explored the influence of Dsp knockdown
391 on hippocampal neurogenesis. First, we examined the effect of Dsp knockdown on cell
392 proliferation. BrdU was administered 2 h before the sacrifice to label proliferating cells
393 (Fig. 4A, left). BrdU-positive cells were detected in the SGZ of the DG (Fig. 4A,
394 middle), and no difference was observed in the number of proliferating cells between
395 the control and Dsp knockdown groups (Fig. 4A, right). We then examined the
396 expression of Neuro D1, which is expressed in progenitors/neuroblasts and immature
397 neurons in the adult DG. The number of NeuroD1-positive cells in the SGZ was
398 significantly decreased in the Dsp knockdown group (Fig. 4B). We further examined
399 the expression of the immature neuronal marker, DCX, in the DG. The total number of
400 DCX-positive cells and those with long dendrites decreased in the Dsp knockdown
401 group (Fig. 4C). Because most newborn cells in the DG die within 2–3 weeks following
402 proliferation in mice (Ueno et al., 2019), we evaluated the effect of Dsp knockdown on
403 the survival of newborn cells 2 weeks after BrdU administration (Fig. 4D, left). The
404 number of BrdU-positive cells in the DG showed a tendency to decrease, yet there was
405 no significant difference between the control group and the Dsp knockdown group (Fig.
406 4D, right).

407

408 **Influence of Dsp knockdown on anxiety-related behaviors**

409 The ventral DG is a key brain region involved in emotional behaviors, including
410 anxiety- and depression-like behaviors (Sahay and Hen, 2007; Levone et al. 2015;

411 Anacker et al. 2018). To examine the influence of Dsp knockdown in the DG on
412 emotion-related behaviors, we conducted three sets of behavioral experiments (Fig. 5A).
413 First, we performed an open-field test to assess behavior in an anxiety-provoking
414 environment. Dsp knockdown in the DG suppressed locomotor activity in the open field
415 box, and a suppressive trend was observed; however, it was not significant for the time
416 spent in the central area or the number of entries into the central area (Fig. 5B). Next,
417 we evaluated immobility time in the FST to assess depression-like behavior. No
418 difference in immobility time between the control and Dsp knockdown groups was
419 observed (Fig. 5C). Another set of experiments was conducted on locomotor activity in
420 a home cage, social interaction test, and elevated plus maze test. Contrary to the data
421 from the open field test, both control and knockdown groups demonstrated comparable
422 locomotor activity under standard conditions (Fig. 5D), suggesting that the knockdown
423 does not perturb baseline locomotor function. In the three-chamber social interaction
424 test, the control mice spent more time around the area with an unfamiliar mouse than
425 around the area with empty cages. This social interaction behavior was comparable to
426 that observed in the Dsp knockdown mice (Fig. 5E). In the elevated plus maze test, a
427 reduction in both the time spent in the open arm and locomotor activity was observed
428 in Dsp knockdown mice (Fig. 5F). These results demonstrate that Dsp knockdown mice
429 in the DG shows anxiety-like behavior. Also, these findings can implicate that
430 expression of Dsp in the DG plays an anti-anxiety role.

Discussion

This study aimed to investigate the role of Dsp expressed in the DG in hippocampal function and emotion-related behaviors. We showed that Dsp is localized mostly in mature granule neurons in the DG and that knockdown of Dsp decreases the expression of neuronal activity marker and serotonin responsiveness in DG neurons while enhancing the expression of mature neuronal markers. In addition, we demonstrated that Dsp knockdown in the DG impairs adult neurogenic processes in the adjacent SGZ and that these hippocampal changes contribute to anxiety-like behaviors. These findings suggest that Dsp in the DG maintains the activity of mature neurons, regulates neuronal differentiation in the adult neurogenic process, and contributes to anxiolytic-like effects. This study is the first to demonstrate the role of Dsp in neuronal activity and emotion-related behaviors in the DG.

Expression of desmoplakin in the DG

Since Dsp could play an important role in cell-to-cell adhesion and subsequent intracellular regulatory signaling, we initially confirmed its localization in the brain. Immunohistological studies showed that Dsp protein was localized in granule cell layer in the DG (Fig. 1B). Dsp colocalized with the NeuN-positive cells, but not with the neural progenitor/immature neuron marker NeuroD1-positive cells in the DG (Fig. 1C). These results are consistent with those of a previous study that demonstrated that Dsp colocalizes with the post-mitotic neuron marker Bcl11b but not with the neural stem cell/progenitor marker SOX2 in the DG at 14 days of age (Simon et al., 2012).

Desmosome components include transmembrane cadherins and intracellular proteins such as plakoglobin, plakophilin, and Dsp (Garrod and Chidgrey, 2008; Broussard et al., 2015). Nevertheless, electron microscopy images of the rat DG showed

456 no desmosome structures between the cell bodies (Laatsch and Cowan, 1966).
457 Therefore, Dsp in the DG may form a complex different from that in epithelial
458 desmosomes. The expression and interactions of each desmosome component in the
459 DG will be examined to elucidate the localization and function of Dsp in neurons.
460

461 **Role of desmoplakin in mature granule neurons in the DG**

462 We found that Dsp knockdown in the DG suppressed FosB expression (Fig. 2D); FosB
463 is useful for monitoring steady-state activation since FosB, including ΔFosB, is induced
464 in response to many types of stimuli and shows high stability (Nestler et al., 1999;
465 Lamothe-Molina et al., 2022). In contrast, Dsp knockdown increased the expression of
466 the mature neuronal markers *Calb1*, *Tdo2*, and *Ntf3* (Fig. 2E), which are negatively
467 regulated by strong neuronal activation, such as in the ECS and epileptic seizures
468 (Imoto et al., 2017; You et al., 2017). Electrophysiological analysis showed that Dsp
469 suppression did not alter the basal transmission efficiency at the MF-CA3 synapses;
470 however, it reduced serotonin-induced potentiation (Fig. 3). Synaptic potentiation by
471 serotonin is mediated by presynaptic 5-HT4 receptor-cAMP signaling in the MF, which
472 is enhanced by antidepressant treatment including ECS (Kobayashi et al., 2008; 2020).
473 Collectively, reduced neuronal response due to Dsp knockdown in the DG may enhance
474 mature marker expression and reduce serotonin-mediated intracellular signaling in the
475 DG.

476 Dsp is involved in various biological processes such as gene expression,
477 differentiation, and cell migration (Bendrick et al., 2018; Dubash et al., 2016; Lombardi
478 et al., 2016; Patel et al., 2014). Dsp interacts with plakoglobin, also known as γ-catenin
479 (Delva et al., 2009). Suppression of Dsp expression in atrial myocyte cell lines leads to
480 nuclear localization of plakoglobin/γ-catenin (Garcia-Gras et al., 2006). Further detail

analysis will be required to characterize the Dsp-mediated transcriptional pathway. Especially, confirmation of the nuclear translocation of plakoglobin/γ-catenin will clarify whether changes in the expression of these factors are mediated by catenin signaling.

Influence of desmoplakin knockdown on the neurogenic process in the DG

Adult neurogenesis in the SGZ of the DG is regulated by various signals from surrounding neurons (Kempermann et al., 2015). We investigated the role of Dsp in several neurogenic processes in the DG. Suppression of Dsp reduced the number of NeuroD1-positive neural progenitors and DCX-positive immature neurons, whereas the number of proliferating cells remained unchanged (Fig. 4). EGFP signals, which should be coexpressed with miRNA, were not observed in DCX-positive cells of the DG (Fig. 2A), suggesting that Dsp in the DG indirectly regulates neurogenic processes in the adjacent SGZ. Forebrain neuron-specific ablation of Dsp impairs hippocampal neurogenesis on postnatal day 14 (Simon et al., 2012). During postnatal development in this mutant line, cell proliferation was suppressed, whereas the number of NeuroD1-positive progenitors increased. All these findings suggest that Dsp is important for the regulation of cell proliferation during developmental neurogenesis and for neural differentiation during both developmental and adult neurogenesis. The reduction in the number of neural progenitors and immature neurons observed in this study may be due to the inhibition of the initial process of neural differentiation or acceleration of the differentiation rate, which allowed them to progress to maturity without sufficient differentiation.

How does Dsp indirectly regulate neuronal differentiation in post-mitotic neurons? Neuronal activation, such as that in the ECS, promotes the expression of adult

506 neurogenic factors such as *Vegf*, *Fgf2*, and *Wnt2* in the DG (Newton et al., 2003;
507 Warner-Schmidt et al., 2007). Conversely, the suppression of neuronal activity in the
508 DG by inhibiting Dsp expression may reduce the expression of these growth factors.
509 Furthermore, intracellular skeletal regulation by Dsp may also affect neurogenic niche
510 formation. The neurogenic niche provides a unique milieu containing an extracellular
511 matrix, humoral factors, and cell-cell contacts that allow controlled neuronal
512 development (Kempermann et al., 2015). Altering the cytoskeleton of dentate granule
513 neurons may affect intercellular contacts and extracellular matrix adhesion and inhibit
514 neurogenic niche formation.
515
516 **Desmoplakin in the DG as a key regulator for emotion-related behaviors**
517 The DG of the hippocampus controls emotion-related behaviors (Segi-Nishida and
518 Suzuki, 2022). Although Dsp knockdown in the DG did not affect baseline locomotor
519 function, depression-like behavior, or social behavior, it reduced the time spent in the
520 open arm in the EPM test and reduced activity in the novel open field and EPM
521 environments designed to elicit anxiety (Fig. 5), indicating an environment-specific
522 anxious-like alteration following Dsp knockdown. The hippocampus plays functionally
523 distinct roles in the dorsal and ventral regions (Fanselow and Dong, 2010). The dorsal
524 region is involved in stress-induced learning and memory changes, and the ventral
525 region contributes to stress responses and emotions such as anxiety. Because AAV was
526 injected into the ventral DG area in this study (as described in the Methods section),
527 Dsp in the ventral DG may play an anxiolytic-like role.
528 In animal models, chronic antidepressant treatment induces anxiolytic-like
529 effects (Santarelli et al., 2003) and promotes the differentiation of newborn neurons in
530 the DG (Wang et al., 2008; Ueno et al., 2019), while suppressing the expression of

531 mature markers, including *Dsp,* in the DG (Fig. 1; Kobayashi et al., 2010; Imoto et al.,
532 2017). The loss of Dsp function in the DG may lead to anxiolytic effects; however,
533 surprisingly, anxiety-like behavior was observed (Fig. 5). Previous findings indicated
534 that adult neurogenesis in the DG affects anxiety-like behaviors. For instance,
535 transgenic mice in which adult neurogenesis was suppressed by the expression of the
536 pro-apoptotic protein BAX in neural progenitor cells show increased anxiety-related
537 behaviors (Revest et al., 2009). Therefore, suppression of adult neurogenesis in the DG
538 by Dsp knockdown may promote anxiety-like behaviors.

539 Furthermore, acute activation of the ventral DG by channelrhodopsin in
540 proopiomelanocortin (POMC)-Cre mice suppresses anxiety-like behavior in the EPM
541 (Kheirbek et al., 2013). Because our findings showed that Dsp knockdown in the DG
542 reduced the expression of the neuronal activity marker FosB (Fig. 2D), the suppression
543 of neuronal activity in the DG by Dsp knockdown may also contribute to anxiety-like
544 behavior.

545 Taken together, our findings demonstrate that Dsp in the DG regulates neuronal
546 function and contributes to anxiolytic-like effects. This research uncovers an
547 unexplored function for Dsp in the central nervous system and implies that Dsp in the
548 DG may function as a regulator maintaining proper neuronal activation. Excessive
549 antidepressant treatment can exacerbate neuronal activation, resulting in increased
550 motor activity (Kobayashi et al., 2010; 2011). Considering the results of these studies
551 and our findings by Dsp knockdown, reduction of Dsp expression by chronic
552 antidepressants in the DG may function as a negative feedback mechanism for
553 excessive neuronal activation rather than merely mediating the effects of
554 antidepressants or anxiolytics.

555

Limitations of the study

First, although we have proposed a role for Dsp in the nervous system, it is not clear what kind of complexes Dsp forms in neurons. In the future, it will be necessary to investigate what kind of factors Dsp binds to and forms complexes with. Second, we do not know how Dsp regulates neuronal activity and neurogenesis; elucidating the regulation of intracellular signaling by Dsp will improve our understanding of neuronal development and function. Third, it is not clear how Dsp in the DG contributes to emotional behaviors and whether Dsp in the DG contributes to learning and memory. The influence of Dsp in the DG on neural circuits involved in emotion needs to be elucidated. In addition, the role of Dsp in the dorsal DG needs to be investigated for its involvement in learning and memory. Finally, this study shows results in male mice only. It is possible that emotion-related behaviors such as anxiety have different phenotypes depending on sex. Future research should also investigate the role of Dsp in the female nervous system.

Acknowledgements: We would like to thank *Editage* (www.editage.jp) for the English language editing.

Data availability statement

All datasets analyzed in the current study are available from the corresponding author upon reasonable request.

Ethics statement

Animal use and procedures were conducted in accordance with the Tokyo University of Science regulations on animal care and use in research and were approved by the Animal Care and Use Committee of Tokyo University of Science (approval number K20009, K21007, and K22007).

Author contributions: KO, NS, YN, YS KK, and KS designed the study, conducted the experiments, analyzed the data, and drafted the manuscript. ESN designed the study, analyzed the data, and drafted the manuscript. All the authors have read and approved the final manuscript.

Funding statements: This work was supported in part by MEXT KAKENHI Grants 20K07090 (ESN), 22K20697 (KS), 23H02801(KK and ESN), and 23K18425(KK). Kato Memorial Bioscience Foundation (KS), Brain Science Foundation (KS), Takeda Science Foundation (KS).

Competing interests: The authors declare no competing interests.

Inclusion and diversity: We support inclusive, diverse, and equitable conduct of research.

References

Allen Institute for Brain Science (2004). Allen Mouse Brain Atlas [https://mouse.brain-map.org/experiment/show/69201504]. Available from mouse.brain-map.org.

Anacker, C., Luna, V.M., Stevens, G.S., Millette, A., Shores, R., Jimenez, J.C., Chen, B., and Hen, R. (2018). Hippocampal neurogenesis confers stress resilience by inhibiting the ventral dentate gyrus. *Nature* 559, 98-102. doi:10.1038/s41586-018-0262-4

Bankhead, P., Loughrey, M.B., Fernandez, J.A., Dombrowski, Y., McArt, D.G., Dunne, P.D., McQuaid, S., Gray, R.T., Murray, L.J., Coleman, H.G., James, J.A., Salto-Tellez, M., and Hamilton, P.W. (2017). QuPath: Open source software for digital pathology image analysis. Sci Rep 7, 16878. doi:10.1038/s41598-017-17204-5

Bendrick, J.L., Eldredge, L.A., Williams, E.I., Haight, N.B., and Dubash, A.D. (2019). Desmoplakin Harnesses Rho GTPase and p38 Mitogen-Activated Protein Kinase Signaling to Coordinate Cellular Migration. *J Invest Dermatol* 139, 1227-1236. doi:10.1016/j.jid.2018.11.032

Broussard, J.A., Getsios, S., and Green, K.J. (2015). Desmosome regulation and signaling in disease. *Cell Tissue Res* 360, 501-512. doi:10.1007/s00441-015-2136-5

Delva, E., Tucker, D.K., and Kowalczyk, A.P. (2009). The desmosome. *Cold Spring Harb Perspect Biol* 1, a002543. doi:10.1101/cshperspect.a002543

Drew, L.J., Fusi, S., and Hen, R. (2013). Adult neurogenesis in the mammalian hippocampus: why the dentate gyrus? *Learn Mem* 20, 710-729. doi:10.1101/lm.026542.112

Dubash, A.D., Kam, C.Y., Aguado, B.A., Patel, D.M., Delmar, M., Shea, L.D., and Green, K.J. (2016). Plakophilin-2 loss promotes TGF-beta1/p38 MAPK-dependent fibrotic gene expression in cardiomyocytes. *J Cell Biol* 212, 425-438. doi:10.1083/jcb.201507018

Fanselow, M.S., and Dong, H.W. (2010). Are the dorsal and ventral hippocampus functionally distinct structures? *Neuron* 65, 7-19. doi:10.1016/j.neuron.2009.11.031

Garcia-Gras, E., Lombardi, R., Giocondo, M.J., Willerson, J.T., Schneider, M.D., Khoury, D.S., and Marian, A.J. (2006). Suppression of canonical Wnt/beta-catenin signaling by nuclear plakoglobin recapitulates phenotype of arrhythmogenic right ventricular cardiomyopathy. *J Clin Invest* 116, 2012-2021. doi:10.1172/JCI27751

Garrod, D., and Chidgey, M. (2008). Desmosome structure, composition and function. *Biochim Biophys Acta* 1778, 572-587. doi:10.1016/j.bbamem.2007.07.014

Imoto, Y., Segi-Nishida, E., Suzuki, H., and Kobayashi, K. (2017). Rapid and stable changes in maturation-related phenotypes of the adult hippocampal neurons by electroconvulsive treatment. *Mol Brain* 10, 8. doi:10.1186/s13041-017-0288-9

Johnson, J.L., Najor, N.A., and Green, K.J. (2014). Desmosomes: regulators of cellular signaling and adhesion in epidermal health and disease. *Cold Spring Harb Perspect Med* 4, a015297. doi:10.1101/cshperspect.a015297

Kempermann, G., Song, H., and Gage, F.H. (2015). Neurogenesis in the Adult Hippocampus. *Cold Spring Harb Perspect Biol* 7, a018812. doi:10.1101/cshperspect.a018812

Kheirbek, M.A., Drew, L.J., Burghardt, N.S., Costantini, D.O., Tannenholz, L., Ahmari, S.E., Zeng, H., Fenton, A.A., and Hen, R. (2013). Differential control of learning and anxiety along the dorsoventral axis of the dentate gyrus. *Neuron* 77, 955-968. doi:10.1016/j.neuron.2012.12.038

Kobayashi, K., Ikeda, Y., Haneda, E., and Suzuki, H. (2008). Chronic fluoxetine bidirectionally modulates potentiating effects of serotonin on the hippocampal mossy fiber synaptic transmission. *J Neurosci* 28, 6272-6280. doi:10.1523/JNEUROSCI.1656-08.2008

Kobayashi, K., Ikeda, Y., Sakai, A., Yamasaki, N., Haneda, E., Miyakawa, T., and Suzuki, H. (2010). Reversal of hippocampal neuronal maturation by serotonergic antidepressants. *Proc Natl Acad Sci U S A* 107, 8434-8439. doi:10.1073/pnas.0912690107

Kobayashi, K., Ikeda, Y., and Suzuki, H. (2011). Behavioral destabilization induced by the selective serotonin reuptake inhibitor fluoxetine. *Mol Brain* 4, 12. doi:10.1186/1756-6606-4-12

Kobayashi, K., Mikahara, Y., Murata, Y., Morita, D., Matsuura, S., Segi-Nishida, E., and Suzuki, H. (2020). Predominant Role of Serotonin at the Hippocampal Mossy Fiber Synapse with Redundant Monoaminergic Modulation. *iScience* 23, 101025. doi:10.1016/j.isci.2020.101025

Kowalczyk, A.P., and Green, K.J. (2013). Structure, function, and regulation of desmosomes. *Prog Mol Biol Transl Sci* 116, 95-118. doi:10.1016/B978-0-12-394311-8.00005-4

Laatsch, R.H., and Cowan, W.M. (1966). Electron microscopic studies of the dentate gyrus of the rat. I. Normal structure with special reference to synaptic organization. *J Comp Neurol* 128, 359-395. doi:10.1002/cne.901280305

Lamothe-Molina, P.J., Franzelin, A., Beck, L., Li, D., Auksutat, L., Fieblinger, T., Laprell, L., Alhbeck, J., Gee, C.E., Kneussel, M., Engel, A.K., Hilgetag, C.C., Morellini, F., and Oertner, T.G. (2022). DeltaFosB accumulation in hippocampal granule cells drives cFos pattern separation during spatial learning. *Nat Commun* 13, 6376. doi:10.1038/s41467-022-33947-w

Levone, B.R., Cryan, J.F., and O'Leary, O.F. (2015). Role of adult hippocampal neurogenesis in stress resilience. *Neurobiol Stress* 1, 147-155. doi:10.1016/j.ynstr.2014.11.003

Lombardi, R., Chen, S.N., Ruggiero, A., Gurha, P., Czernuszewicz, G.Z., Willerson, J.T., and Marian, A.J. (2016). Cardiac Fibro-Adipocyte Progenitors Express Desmosome Proteins and Preferentially Differentiate to Adipocytes Upon Deletion of the Desmoplakin Gene. *Circ Res* 119, 41-54. doi:10.1161/CIRCRESAHA.115.308136

Nestler, E.J., Kelz, M.B., and Chen, J. (1999). DeltaFosB: a molecular mediator of long-term neural and behavioral plasticity. *Brain Res* 835, 10-17. doi:10.1016/s0006-8993(98)01191-3

Newton, S.S., Collier, E.F., Hunsberger, J., Adams, D., Terwilliger, R., Selvanayagam, E., and Duman, R.S. (2003). Gene profile of electroconvulsive seizures: induction of neurotrophic and angiogenic factors. *J Neurosci* 23, 10841-10851. doi:10.1523/JNEUROSCI.23-34-10841.2003

Patel, D.M., Dubash, A.D., Kreitzer, G., and Green, K.J. (2014). Disease mutations in desmoplakin inhibit Cx43 membrane targeting mediated by desmoplakin-EB1 interactions. *J Cell Biol* 206, 779-797. doi:10.1083/jcb.201312110

Paxinos, G.F., K. B. J., 2012. 4th ed. Academic Press., Cambridge, MA.

Rao, S., Kay, Y., and Herring, B.E. (2019). Tiam1 is Critical for Glutamatergic Synapse Structure and Function in the Hippocampus. *J Neurosci* 39, 9306-9315. doi:10.1523/JNEUROSCI.1566-19.2019

Revest, J.M., Dupret, D., Koehl, M., Funk-Reiter, C., Grosjean, N., Piazza, P.V., and Abrous, D.N. (2009). Adult hippocampal neurogenesis is involved in anxiety-related behaviors. *Mol Psychiatry* 14, 959-967. doi:10.1038/mp.2009.15

Sahay, A., and Hen, R. (2007). Adult hippocampal neurogenesis in depression. *Nat Neurosci* 10, 1110-1115. doi:10.1038/nn1969

Santarelli, L., Saxe, M., Gross, C., Surget, A., Battaglia, F., Dulawa, S., Weisstaub, N., Lee, J., Duman, R., Arancio, O., Belzung, C., and Hen, R. (2003). Requirement of hippocampal neurogenesis for the behavioral effects of antidepressants. *Science* 301, 805-809. doi:10.1126/science.1083328

Segi-Nishida, E., and Suzuki, K. (2022). Regulation of adult-born and mature neurons in stress response and antidepressant action in the dentate gyrus of the hippocampus. *Neurosci Res*. doi:10.1016/j.neures.2022.08.010

Sehara, Y., Hayashi, Y., Ohba, K., Uchibori, R., Urabe, M., Inutsuka, A., Shimazaki, K., Kawai, K., and Mizukami, H. (2022). Higher Transduction Efficiency of AAV5 to Neural Stem Cells and Immature Neurons in Gerbil Dentate Gyrus Compared to AAV2 and rh10. *Hum Gene Ther* 33, 76-85. doi:10.1089/hum.2021.106

Shinohara, R., Taniguchi, M., Ehrlich, A.T., Yokogawa, K., Deguchi, Y., Cherasse, Y., Lazarus, M., Urade, Y., Ogawa, A., Kitaoka, S., Sawa, A., Narumiya, S., and Furuyashiki, T. (2018). Dopamine D1 receptor subtype mediates acute stress-induced dendritic growth in excitatory neurons of the medial prefrontal cortex and contributes to suppression of stress susceptibility in mice. *Mol Psychiatry* 23, 1717-1730. doi:10.1038/mp.2017.177

Simon, R., Brylka, H., Schwegler, H., Venkataramanappa, S., Andratschke, J., Wiegreffe, C., Liu, P., Fuchs, E., Jenkins, N.A., Copeland, N.G., Birchmeier, C., and Britsch, S. (2012). A dual function of Bcl11b/Ctip2 in hippocampal neurogenesis. *EMBO J* 31, 2922-2936. doi:10.1038/emboj.2012.142

Ueno, M., Sugimoto, M., Ohtsubo, K., Sakai, N., Endo, A., Shikano, K., Imoto, Y., and Segi-Nishida, E. (2019). The effect of electroconvulsive seizure on survival, neuronal differentiation, and expression of the maturation marker in the adult mouse hippocampus. *J Neurochem* 149, 488-498. doi:10.1111/jnc.14691

Wang, J.W., David, D.J., Monckton, J.E., Battaglia, F., and Hen, R. (2008). Chronic fluoxetine stimulates maturation and synaptic plasticity of adult-born hippocampal granule cells. *J Neurosci* 28, 1374-1384. doi:10.1523/JNEUROSCI.3632-07.2008

Warner-Schmidt, J.L., and Duman, R.S. (2007). VEGF is an essential mediator of the neurogenic and behavioral actions of antidepressants. *Proc Natl Acad Sci U S A* 104, 4647-4652. doi:10.1073/pnas.0610282104

Yamasaki, N., Maekawa, M., Kobayashi, K., Kajii, Y., Maeda, J., Soma, M., Takao, K., Tanda, K., Ohira, K., Toyama, K., Kanzaki, K., Fukunaga, K., Sudo, Y., Ichinose, H., Ikeda, M., Iwata, N., Ozaki, N., Suzuki, H., Higuchi, M., Suhara, T., Yuasa, S., and Miyakawa, T. (2008). Alpha-CaMKII deficiency causes immature dentate gyrus, a novel candidate endophenotype of psychiatric disorders. *Mol Brain* 1, 6. doi:10.1186/1756-6606-1-6

You, J.C., Muralidharan, K., Park, J.W., Petrof, I., Pyfer, M.S., Corbett, B.F., LaFrancois, J.J., Zheng, Y., Zhang, X., Mohila, C.A., Yoshor, D., Rissman, R.A., Nestler, E.J., Scharfman, H.E., and Chin, J. (2017). Epigenetic suppression of hippocampal calbindin-D28k by DeltaFosB drives seizure-related cognitive deficits. *Nat Med* 23, 1377-1383. doi:10.1038/nm.4413

Zhao, C., Deng, W., and Gage, F.H. (2008). Mechanisms and functional implications of adult neurogenesis. *Cell* 132, 645-660. doi:10.1016/j.cell.2008.01.033

Figure legends

Figure 1. Expression of Dsp in the dentate gyrus (DG) of the hippocampus

(A) Expression of Dsp mRNA in adult mouse brain from Allen Mouse Brain Atlas. (B) Low magnification images of immunoreactivity for Dsp (magenta) in the DG and CA1. DAPI (cyan) is utilized for nuclear staining. GCL; granule cell layer, ML; molecular layer. Scale bar: 200 μm. (C) Representative images of immunoreactivity for Dsp (green), NeuN (upper, magenta), and NeuroD1 (lower, magenta) in the DG. DAPI was used for nuclear staining (blue). Enlarged images of the dotted square are shown below. Arrows represent Dsp-negative and NeuroD1-positive cells (arrows). Scale bars: 50 μm. (D) Relative gene expression of *Dsp* at 24 h after 11 times of electroconvulsive seizure (ECS) stimulation (left) or 4-weeks treatment of selective serotonin reuptake inhibitor (SSRI) fluoxetine (right). Data are expressed using dot plots and means ± standard error of mean. The n number is given in graph. *, $P<0.05$; **, $P<0.01$. Detailed statistical data are shown in Table 2. (E) Representative images of immunoreactivity for Dsp (green) in the DG after 20 times of ECS stimulation. Scale bars: 20 μm.

Figure 2. Knockdown of Dsp in the DG by adeno-associated virus (AAV) carrying Dsp artificial miRNA and expression changes in the DG

(A) Structure of AAVrh10 carrying EGFP and artificial microRNA sequence for Dsp (DSP miRNA) and time course of experimental procedure. Representative EGFP image 7–8 weeks after control miRNA AAV injection into the DG (left). EGFP and immunoreactivity for an immature neuronal marker doublecortin (magenta) in the DG (right). (B) Gene expression of *Dsp* 7–8 weeks after AAV infection. (C) Representative images of immunoreactivity for Dsp (red) and DAPI (blue) in the DG after AAV infection. (D) Effect of Dsp knockdown in the DG on the expression of FosB protein.

770 Representative images of immunoreactivity for FosB in the DG (left). Quantification
771 of FosB-positive cell numbers (right) in the granule cell layer. (E) Effect of Dsp
772 knockdown in the DG on the expression of DG specific maturation markers in the DG.
773 Expression of *Calb1, Tdo2, Ntf3,* and *Il1r1*. Data are expressed using dot plots and
774 means ± standard error of mean. The n number is given in graph. *, $P<0.05$; **, $P<0.01$;
775 ***, $P<0.001$; n.s., not significant. Detailed statistical data are shown in Table 2. Scale
776 bars: 1 mm for the low magnification image in Fig. 1A (left); 100 μm for other images.
777

778 **Figure 3. Electrophysiological changes in the DG by Dsp knockdown**

779 (A) Diagram showing the electrode arrangement for recording field excitatory post
780 synaptic potentials (EPSPs) at the mossy fiber (MF)–CA3 synapse. (B) Ratios for MF
781 field EPSPs to fiber volley (FV) at the baseline stimulus intensity. (C and D) Effect of
782 Dsp knockdown on synaptic facilitation induced by repetitive stimulation at the MF
783 synapse. (E) Effect of Dsp knockdown on potentiation of MF synaptic transmission
784 induced by serotonin (5 μM, 5 min) applied in the bath. Sample recordings show
785 averages of nine consecutive field EPSPs before and at the end of serotonin application
786 in control DG and knockdown DG. (F) Effect of Dsp knockdown on serotonin-induced
787 synaptic potentiation. Data are expressed using dot plots and means ± standard error of
788 mean. The n number of data is given in graph and represents the number of slices. **,
789 $P<0.01$. Detailed statistical data are shown in Table 2.
790

791 **Figure 4. Adult neurogenic changes in the DG by Dsp knockdown**

792 (A) Effect of Dsp knockdown on proliferation in the DG. Left: Time course of the
793 experimental procedure. Middle: Representative images of immunoreactivity for BrdU
794 (red). The arrows represent BrdU-positive cells in the SGZ. Scale bars: 20 μm. Right:

795 Quantification of BrdU-positive cell numbers in the SGZ. (B) Effect of Dsp knockdown
796 on neuronal differentiation in the DG. Left: Representative images of immunoreactivity
797 for NeuroD1 in the DG. Scale bars: 100 μm. Right: Quantification of NeuroD1-positive
798 cell numbers in the SGZ. (C) Effect of Dsp knockdown on cell number of doublecortin
799 (DCX)-positive immature neurons in the DG. Left: Representative images of
800 immunoreactivity for DCX in the DG. Scale bars: 40 μm. Middle: Quantification of
801 DCX-positive cell numbers in the SGZ. Right: Quantification of DCX-positive cells
802 with long dendrites in the SGZ. (D) Effect of Dsp knockdown on survival of 2-weeks
803 of cell age in the DG. Left: Time course of the experimental procedure. Right:
804 Quantification of BrdU-positive cells of 2-weeks (2 wks) of cell age in the DG. Data
805 are expressed using dot plots and means ± standard error of mean. The n number is
806 given in graph. *, $P<0.05$; **, $P<0.01$. n.s. not significant. Detailed statistical data are
807 shown in Table 2.
808
809 **Figure 5. Behavioral changes in the DG by Dsp knockdown**
810 (A) Time course of the experimental procedure. (B) Exploratory behaviors of open field
811 test (OFT). Total distance (left) in the open field. Time spent (middle) and entry times
812 (right) in the center of the open field. (C) Immobility time in the forced swim test (FST).
813 (D) Total distance of locomotor activity (LMA) in the home cage. (E) Social interaction
814 behavior in the 3-chamber social interaction test (SIT). A stranger mouse within a wire
815 cup placed in one chamber (social) and an empty wire cup placed in another chamber
816 (Non-Social). (F) Time spent on the open arms (left) and total distance (right) in the
817 elevate plus maze (EPM) test. Data are expressed using dot plots and means ± standard
818 error of mean. The n number is given in graph. *, $P<0.05$; **, $P<0.01$; n.s. not
819 significant. Detailed statistical data are shown in Table 2.

Table 1. List of primers used for qPCR analysis.

Gene	Forward (5' to 3')	Reverse (5' to 3')
Dsp	GCTGAAGAACACTCTAGCCCA	ACTGCTGTTTCCTCTGAGACA
Calb1	TCTGGCTTCATTTCGACGCTG	ACAAAGGATTTCATTTCCGGTGA
Tdo2	ATGAGTGGGTGCCCGTTTG	GGCTCTGTTTACACCAGTTTGAG
Ntf3	AGTTTGCCGGAAGACTCTCTC	GGGTGCTCTGGTAATTTTCCTTA
Il1r1	GTGCTACTGGGGCTCATTTGT	GGAGTAAGAGGACACTTGCGAAT
Hdac2	GGAGGAGGCTACACAATCCG	TCTGGAGTGTTCTGGTTTGTCA
Tiam1	AGACTGAACGCACCTATGTGA	ACTCGACTTGAAACTCCACCAT
18S	GAGGCCCTGTAATTGGAATGAG	GCAGCAACTTTAATATACGCTATTGG
Gapdh	AGGTCGGTGTGAACGGATTTG	TGTAGACCATGTAGTTGAGGTCA

Table 2. Statistical analysis

		F value	Statistical Test	T value	P value
Figure 1D; *Dsp*	CNT, n=3 ECS, n=4	F(2,3)=22.92, P=0.0304	Unpaired t test with Welch's correction	t(5.504)=2.131	P=0.0324
Figure 1D; *Dsp*	CNT, n=7 SSRI, n=7	F(6,6)=7.606, P=0.0262	Unpaired t test with Welch's correction	t(7.551)=3.818	P=0.0057
Figure 2B; *Dsp*	CNT, n=9 KD, n=9	F(8,8)=6.584, P=0.0152	Unpaired t test with Welch's correction	t(10.38)=2.239	P=0.0482
Figure 2D; FosB(+)	CNT, n=4 KD, n=3	F(3,2)=1.636, P=0.8023	Unpaired t test	t(5)=10.17	P=0.0002
Figure 2E; *Calb*	CNT, n=8 KD, n=9	F(7,6)=3.495, P=0.1485	Unpaired t test	t(13)=2.572	P=0.0232
Figure 2E; *Tdo2*	CNT, n=7 KD, n=8	F(7,6)=4.257, P=0.0974	Unpaired t test	t(13)=2.662	P=0.0195
Figure 2E; *Ntf3*	CNT, n=9 KD, n=9	F(8,8)=1.275, P=0.7396	Unpaired t test	t(16)=3.373	P=0.00039
Figure 2E; *Il1r1*	CNT, n=9 KD, n=9	F(8,8)=1.006, P=0.9933	Unpaired t test	t(16)=0.5359	P=0.5926
Figure 3B; EPSP/FV	CNTDG,n=9 KD DG, n=9	F(8,8)=1.362, P=0.6994	Unpaired t test	t(16)=0.9823	P=0.3406
Figure 3D; 1Hz facilitation	CNTDG,n=7 KDDG n=7	F(6,6)=2.402, P=0.3104	Unpaired t test	t(12)=0.07857	P=0.9387
Figure 3F; serotonin	CNTDG,n=5 KDDG, n=5	F(4,4)=2.407, P=0.4158	Unpaired t test	t(8)=4.158	P=0.0032
Figure 4A; proliferation	CNT, n=7 KD, n=5	F(6,4)=3.905, P=0.2083	Unpaired t test	t(10)=0.5153	P=0.6175
Figure 4B; NeuroD1(+)	CNT, n=6 KD, n=6	F(5,5)=4.677, P=0.1157	Unpaired t test	t(10)=4.338	P=0.0015

Figure 4C; DCX(+)	CNT, n=5 KD, n=6	F(4,5)=6.073, P=0.0740	Unpaired t test	t(9)=3.001	P=0.0149
Figure 4C; long-DCX(+)	CNT, n=5 KD, n=6	F(4,5)=7.397, P=0.0499	Unpaired t test with Welch's correction	t(4.902)=2.833	P=0.0374
Figure 4D; survival	CNT, n=5 KD, n=6	F(4,5)=1.843, P=0.5170	Unpaired t test	t(9)=1.486	P=0.1715
Figure 5B; OFT, distance	CNT, n=8 KD, n=11	F(6,5)=1.051, P=0.9769	Unpaired t test	t(11)=4.010	P=0.0021
Figure 5B; OFT, center	CNT, n=8 KD, n=11		Mann-Whitney test	U=24	P=0.1087
Figure 5B; OFT, entry	CNT, n=8 KD, n=11		Mann-Whitney test	U=23.5	P=0.0936
Figure 5C; FST	CNT, n=7 KD, n=8	F(6,7)=2.652, P=0.2279	Unpaired t test	t(13)=0.6832	P=0.5065
Figure 5D; LMA	CNT, n=18 KD, n=17	F(17,16)=1.416, P=0.4915	Unpaired t test	t(33)=0.9365	P=0.3558
Figure 5E; SIT time in zone	CNT, n=17 KD, n=15	Two-way ANOVA	interaction	F(1,60)=0.5081	P=0.4787
			knockdown	F(1,60)=0.2990	P=0.5865
			social state	F(1,60)=41.97	P<0.0001
Figure 5F; EPM, Open	CNT, n=18 KD, n=17	F(17,16)=2.849, P=0.0419	Unpaired t test with Welch's correction	t(27.89)=2.054	P=0.0495
Figure 5F; EPM, Distance	CNT, n=18 KD, n=17	F(17,16)=1.683 P=0.3043	Unpaired t test	t(33)=2.329	P=0.0262

828 **Key resources table**

REAGENT or RESOURCE	SOURCE	IDENTIFIER
Antibodies		
Mouse monoclonal anti-Desmoplakin 1+2	Progen	Cat# 61003, RRID: AB_2920666
Rabbit monoclonal anti-NeuN	abcam	Cat# ab177487, RRID: AB_2532109
Rabbit monoclonal anti-NeuroD1	abcam	Cat# ab213725, RRID: AB_2801303
Rabbit monoclonal anti-FosB	abcam	Cat# ab184938, RRID: AB_2721123
Rat monoclonal anti-BrdU	abcam	Cat# ab6326, RRID: AB_305426
Rabbit polyclonal anti-Doublecortin	Cell signaling	Cat# 4604, RRID: AB_561007
Donkey anti-Mouse IgG (H+L) Highly Cross-Adsorbed Secondary Antibody, Alexa Fluo 488	Thermo Fisher Scientific,	Cat# A21202 RRID: AB_141607
Donkey anti-Rabbit IgG (H+L) Highly Cross-Adsorbed Secondary Antibody, Alexa Fluor 555	Thermo Fisher Scientific	Cat# A31572 RRID: AB_162543
Rabbit anti-Mouse IgG (H+L) Cross-Adsorbed Secondary Antibody, Alexa Fluo 555	Thermo Fisher Scientific	Cat# A21427 RRID: AB_2535848
Donkey Anti-Rat IgG H&L (Alexa Fluor® 555) preadsorbed	abcam	Cat# ab150154, RRID: AB_2813834
Goat anti-Rabit IgG antibody (H+L), Biotinylated	Vector Laboratories	Cat# BA-1000 RRID: AB_2313606
Bacterial and virus strains		
AAV-EF1α-EmGFP-miR-Dsp	This paper	N/A
AAV-EF1α-EmGFP-miR-Control	This paper	N/A
Chemicals, peptides, and recombinant proteins		
DAPI	Sigma	Cat# D9542
Lipofectamine 2000	Thermo Fisher Scientific	Cat# 11668027
Benzonase	Merck Millipore	Cat# 71205-3CN
Rever Tra Ace qPCR RT Master Mix	TOYOBO	Cat# FSQ-201
THUNDERBIRD SYBR qPCR Mix	TOYOBO	Cat# QPS-201
DCG-IV	Tocris Bioscience	Cat# 0975
BrdU	Nacalai Tesque	Cat# 05650
Critical commercial assays		
BLOCK-iT Pol II miR RNAi Expression Vector Kit	Thermo Fisher Scientific	Cat# K493600
Reliaprep RNA Cell Miniprep System	Promega	Cat# Z6010
Vectastain Elite ABC Standard kit	Vector Laboratories	Cat#PK-6101
Experimental models: Cell lines		
AAV-293 cells	Agilent	Cat#240073
Experimental models: Organisms/strains		
Mouse: C57BL/6N	SLC	RRID: MGI:5295404
Oligonucleotides		
qPCR primers	This paper	See Table S1
Forward primer for AAV titer 5'-TGA GTC ACC CAC ACA AAG GA-3′	This paper	N/A

Reverse primer for AAV titer 5-CCA AGC TGG CCT AAC TTC AG-3′	This paper	N/A
Recombinant DNA		
pAAV-EF1α-EmGFP-miR-Dsp	This paper	N/A
pAAV-EF1α-EmGFP-miR-Control	This paper	N/A
AAVrh10	Addgene	Cat# 112866
pHelper	Agilent Technologies	Cat# 240071
Software and algorithms		
Fiji / ImageJ	NIH	https://imagej.nih.gov/ij/
QuPath	Bankhead et al., (2017)	RRID:SCR_018257
Step One	Applied Biosystem	RRID: SCR_014281
SMART 3.0	Panlab	RRID: SCR_002852
GraphPad Prism 9	GraphPad Software	RRID: SCR_002798

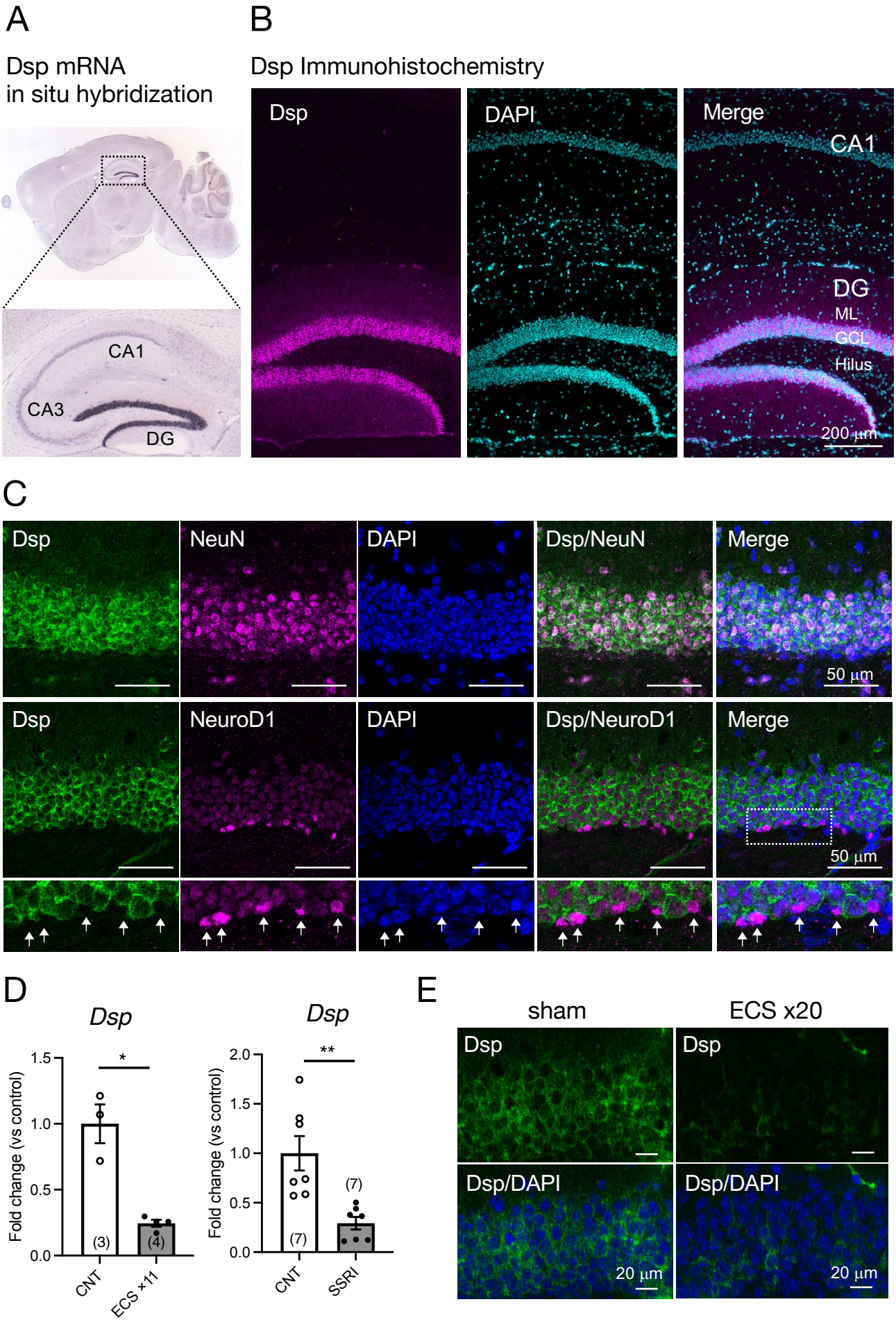
A
Dsp mRNA
in situ hybridization
CA1
CA3
DG
B
Dsp Immunohistochemistry
Dsp
DAPI
Merge
CA1
DG
ML
GCL
Hilus
200 µm
C
Dsp
NeuN
DAPI
Dsp/NeuN
Merge
50 µm
Dsp
NeuroD1
DAPI
Dsp/NeuroD1
Merge
50 µm
D
Dsp
Fold change (vs control)
1.5
1.0
0.5
0.0
*
(3)
(4)
CNT
ECS x11
Dsp
2.0
1.5
1.0
0.5
0.0
**
(7)
(7)
CNT
SSRI
E
sham
ECS x20
Dsp
Dsp
Dsp/DAPI
Dsp/DAPI
20 µm
20 µm

Figure 1

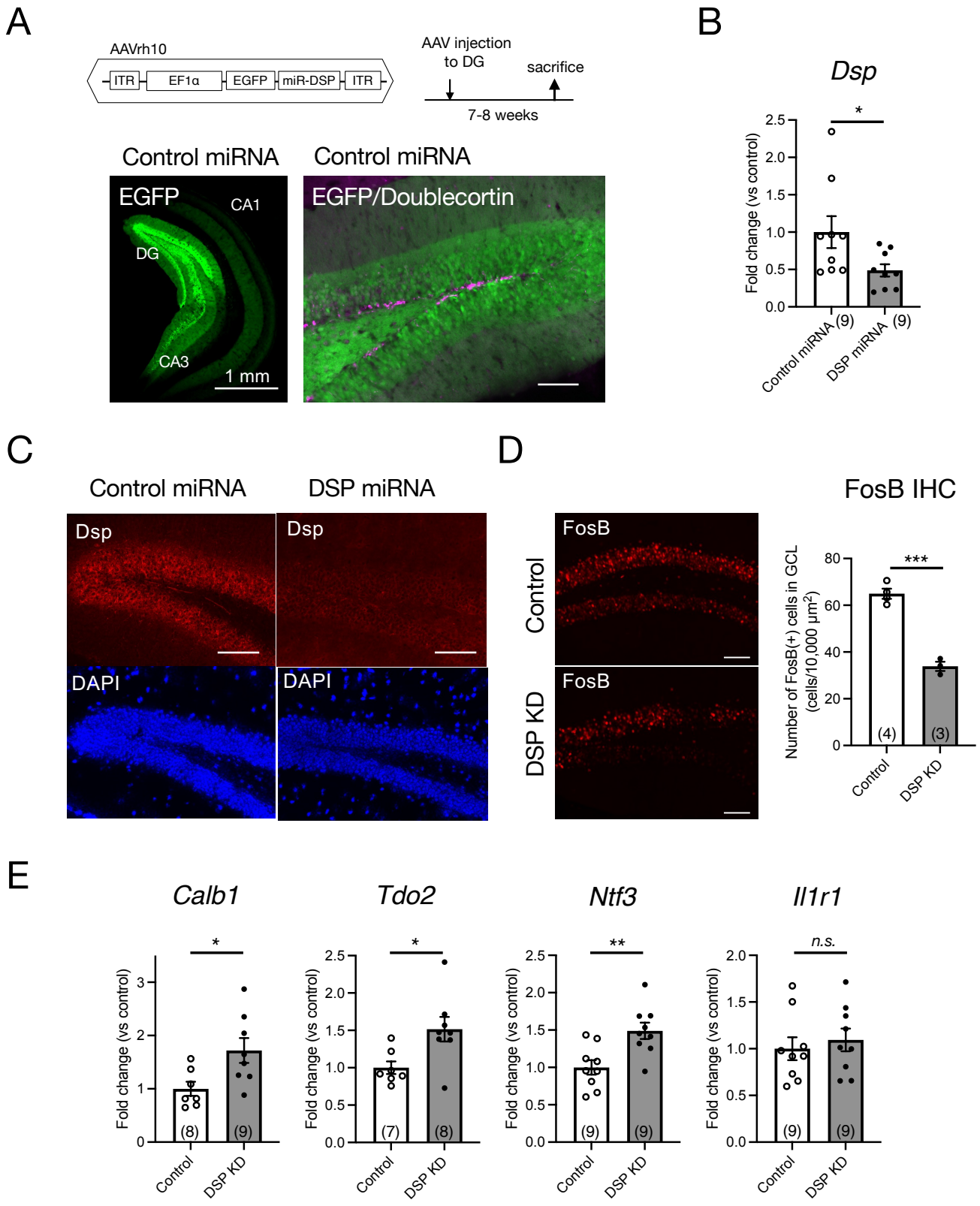
A
AAVrh10
ITR
EF1α
EGFP
miR-DSP
ITR
AAV injection to DG
sacrifice
7-8 weeks
Control miRNA
Control miRNA
EGFP
CA1
DG
CA3
1 mm
EGFP/Doublecortin
B
Dsp
Fold change (vs control)
Control miRNA
DSP miRNA
(9)
(9)
C
Control miRNA
DSP miRNA
Dsp
Dsp
DAPI
DAPI
D
FosB IHC
Control
DSP KD
FosB
FosB
Number of FosB(+) cells in GCL (cells/10,000 μm²)
Control
DSP KD
(4)
(3)
E
Calb1
Tdo2
Ntf3
Il1r1
Fold change (vs control)
n.s.
Control
DSP KD
(8)
(9)
(7)
(8)
(9)
(9)
(9)
(9)

Figure 2

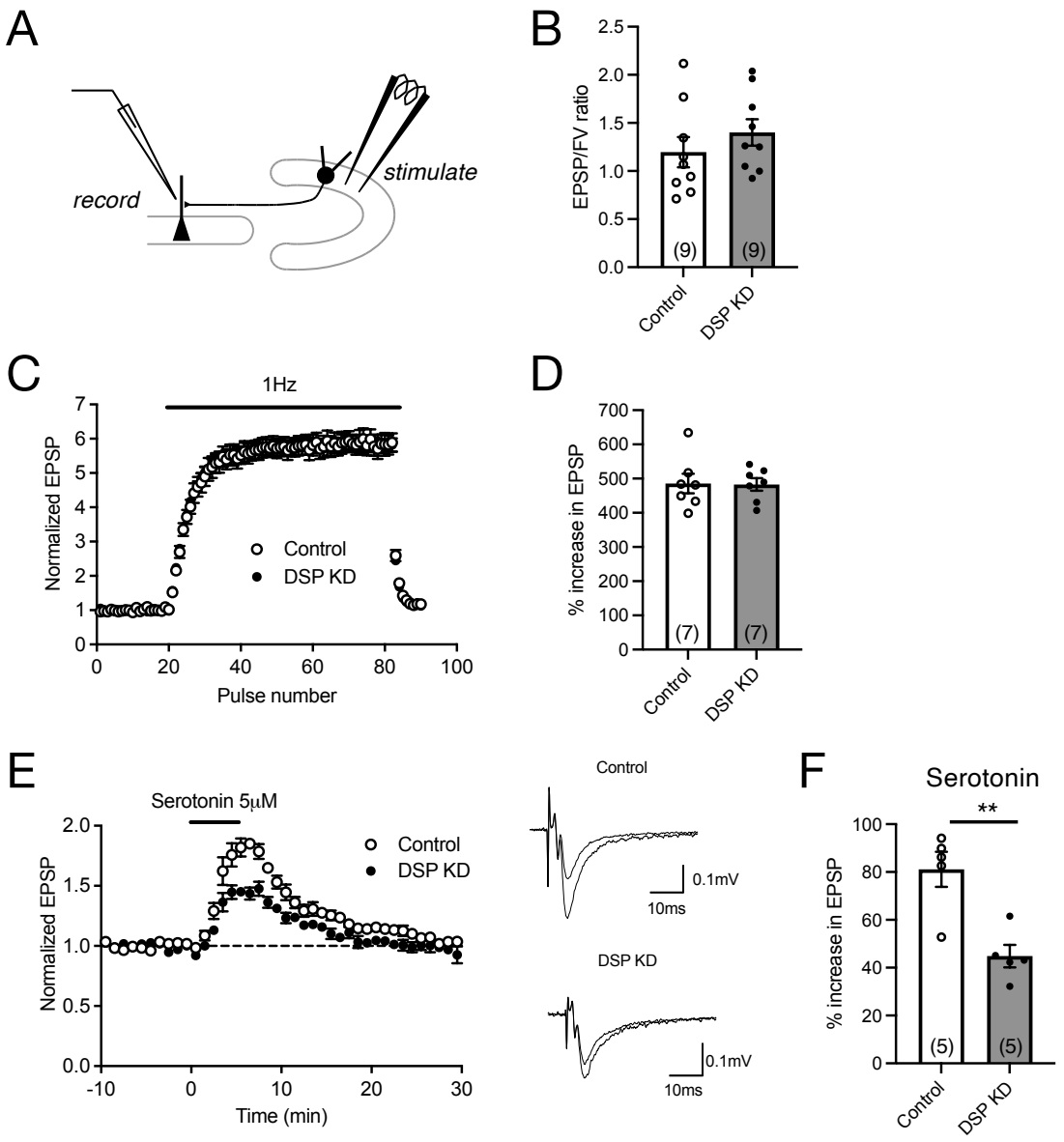
A
record
stimulate
B
EPSP/FV ratio
2.5
2.0
1.5
1.0
0.5
0.0
(9)
(9)
Control
DSP KD
C
1Hz
Normalized EPSP
7
6
5
4
3
2
1
0
Control
DSP KD
0
20
40
60
80
100
Pulse number
D
% increase in EPSP
700
600
500
400
300
200
100
0
(7)
(7)
Control
DSP KD
E
Serotonin 5μM
Normalized EPSP
2.0
1.5
1.0
0.5
0.0
Control
DSP KD
-10
0
10
20
30
Time (min)
Control
0.1mV
10ms
DSP KD
0.1mV
10ms
F
Serotonin
**
% increase in EPSP
100
80
60
40
20
0
(5)
(5)
Control
DSP KD

Figure 3

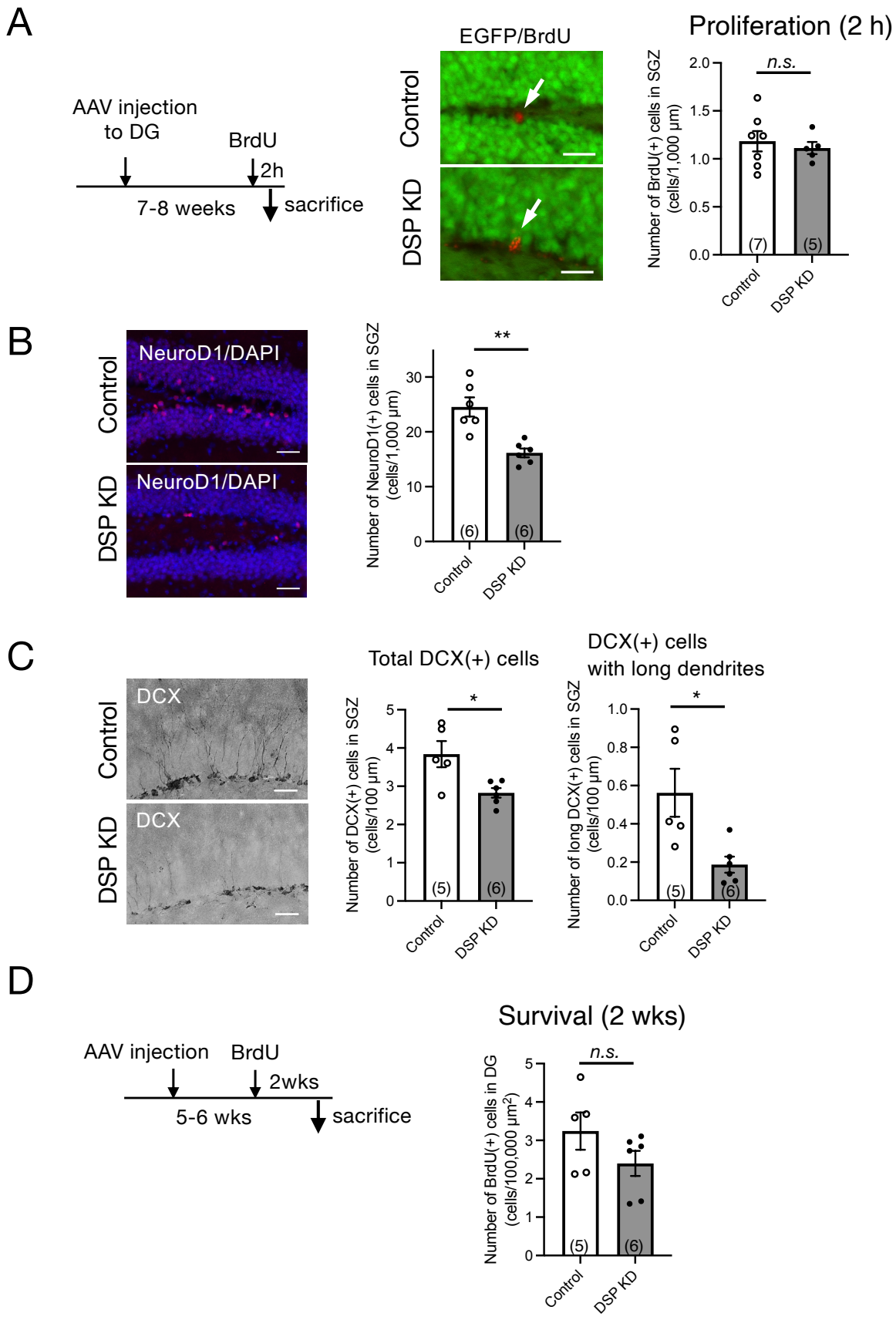
A
AAV injection
to DG
BrdU
2h
7-8 weeks
sacrifice
EGFP/BrdU
Control
DSP KD
Proliferation (2 h)
n.s.
Number of BrdU(+) cells in SGZ
(cells/1,000 μm)
2.0
1.5
1.0
0.5
0.0
(7)
(5)
Control
DSP KD
B
NeuroD1/DAPI
Control
NeuroD1/DAPI
DSP KD
**
Number of NeuroD1(+) cells in SGZ
(cells/1,000 μm)
30
20
10
0
(6)
(6)
Control
DSP KD
C
DCX
Control
DCX
DSP KD
Total DCX(+) cells
*
Number of DCX(+) cells in SGZ
(cells/100 μm)
5
4
3
2
1
0
(5)
(6)
Control
DSP KD
DCX(+) cells
with long dendrites
*
Number of long DCX(+) cells in SGZ
(cells/100 μm)
1.0
0.8
0.6
0.4
0.2
0.0
(5)
(6)
Control
DSP KD
D
AAV injection
BrdU
2wks
5-6 wks
sacrifice
Survival (2 wks)
n.s.
Number of BrdU(+) cells in DG
(cells/100,000 μm²)
5
4
3
2
1
0
(5)
(6)
Control
DSP KD

Figure 4

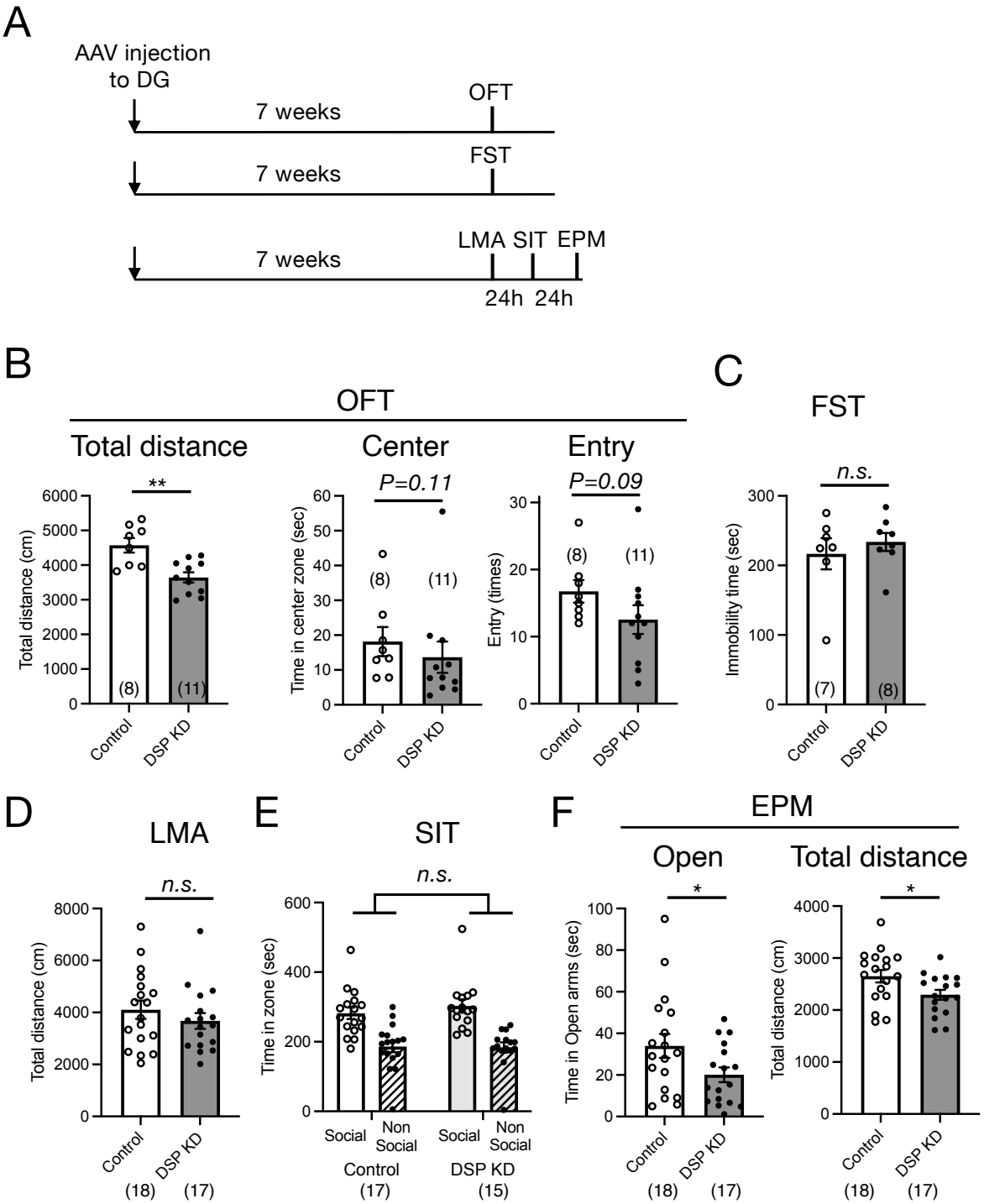
A
AAV injection
to DG
7 weeks
OFT
7 weeks
FST
7 weeks
LMA SIT EPM
24h 24h
B
OFT
Total distance
Center
Entry
**
P=0.11
P=0.09
Total distance (cm)
Time in center zone (sec)
Entry (times)
(8)
(11)
Control
DSP KD
C
FST
n.s.
Immobility time (sec)
(7)
(8)
D
LMA
n.s.
Total distance (cm)
(18)
(17)
E
SIT
n.s.
Time in zone (sec)
Social
Non Social
Control
DSP KD
(17)
(15)
F
EPM
Open
Total distance
*
Time in Open arms (sec)
Total distance (cm)
(18)
(17)

Figure 5